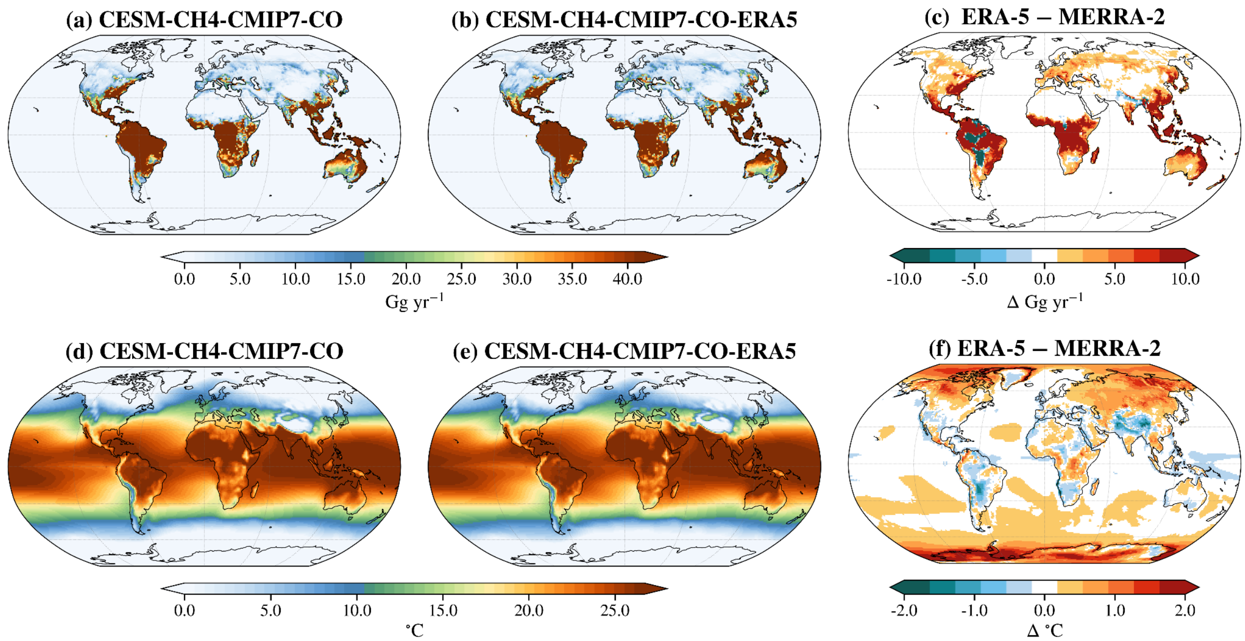

Figure S1. Annual-mean (2003–2022) maps of biogenic isoprene emission (top row) and surface temperature (bottom row) from two configurations that share identical emissions but differ in the meteorological reanalysis used for nudging: CESM-CH4-CMIP7-CO, driven by MERRA-2 (a, d), and CESM-CH4-CMIP7-CO-ERA5, driven by ERA-5 (b, e), together with their difference (ERA-5 − MERRA-2; c, f)

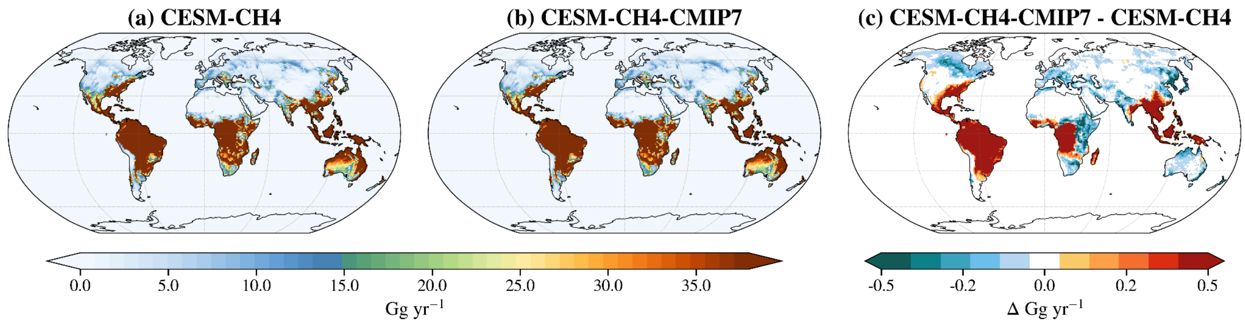

Figure S2. Annual-mean (2003–2022) biogenic isoprene emission (Gg yr^{-1}) for two configurations that share MERRA-2 meteorology but use different chemical-emission inventories: CESM-CH4 (CAMS + FINN, a) and CESM-CH4-CMIP7 (CMIP7/CEDS, b), together with their difference (CESM-CH4-CMIP7 − CESM-CH4; c).

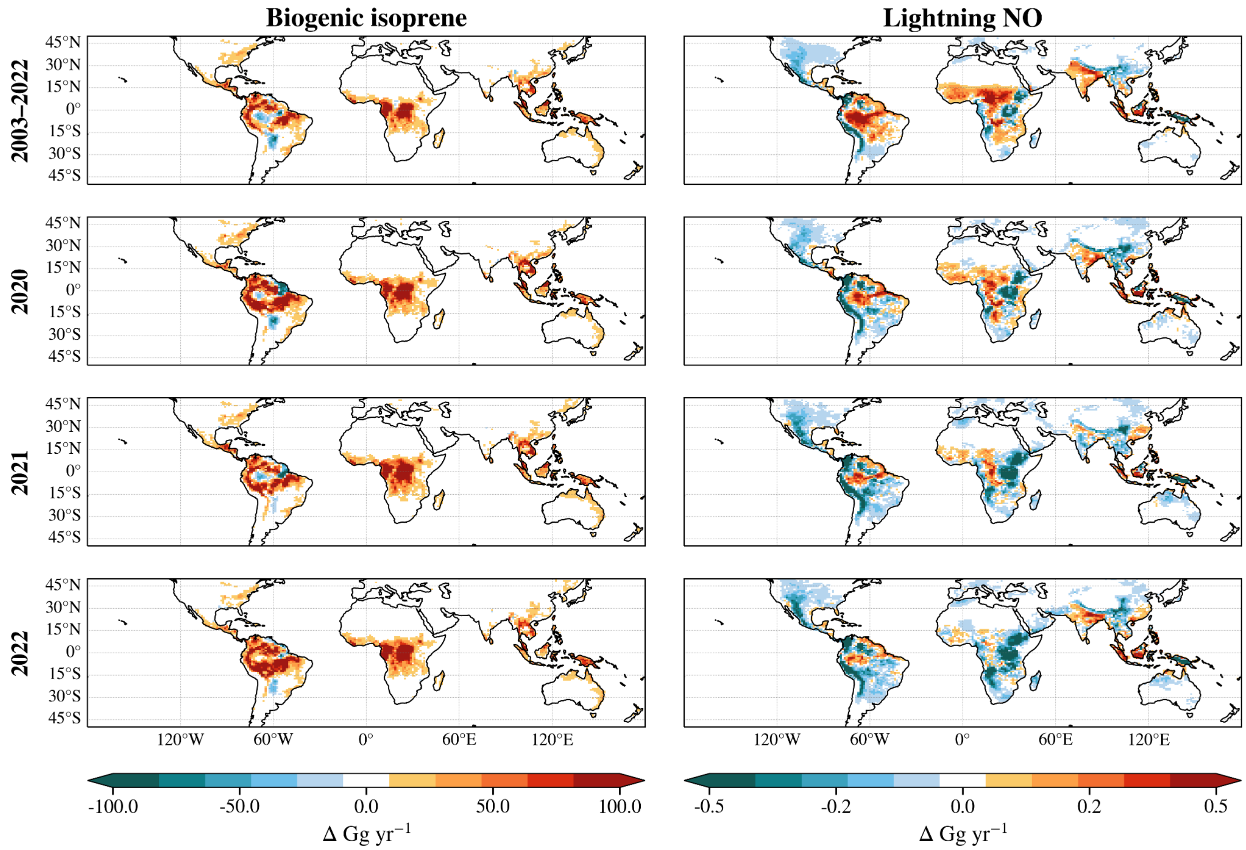

Figure S3. Differences in annual biogenic isoprene (left) and lightning NO (right) emission between the ERA5- and MERRA-2-driven runs (CESM-CH4-CMIP7-CO-ERA5 − CESM-CH4-CMIP7-CO).

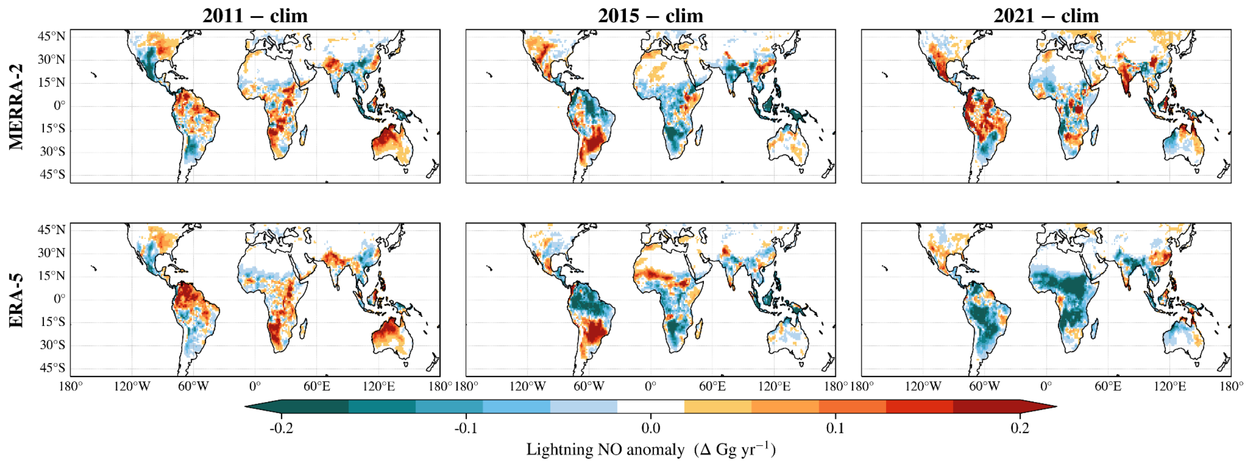

Figure S4. Lightning NO emission anomalies (individual year minus the 2003–2022 climatology) for three ENSO years, the La Niña years 2011 and 2021 and the strong El Niño year 2015, for the MERRA-2-driven simulation CESM-CH4-CMIP7-CO (top row) and the ERA-5-driven simulation CESM-CH4-CMIP7-CO-ERA5 (bottom row).

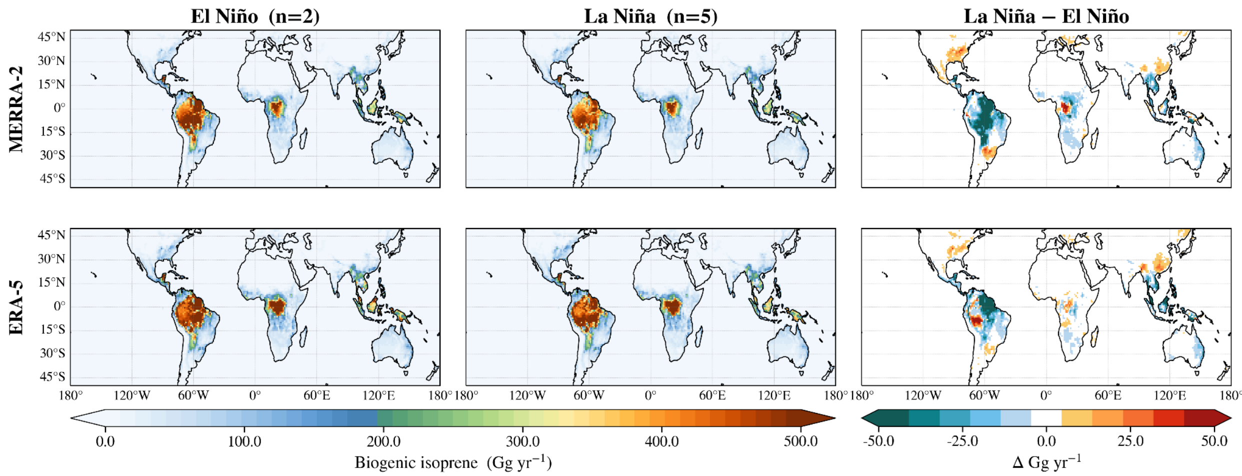

Figure S5. Biogenic isoprene emission (Gg yr^{-1}) averaged separately over El Niño years (2004 and 2015) and La Niña years (2007, 2008, 2011, 2021 and 2022), for the MERRA-2-driven simulation CESM-CH4-CMIP7-CO (top row) and the ERA-5-driven simulation CESM-CH4-CMIP7-CO-ERA5 (bottom row).

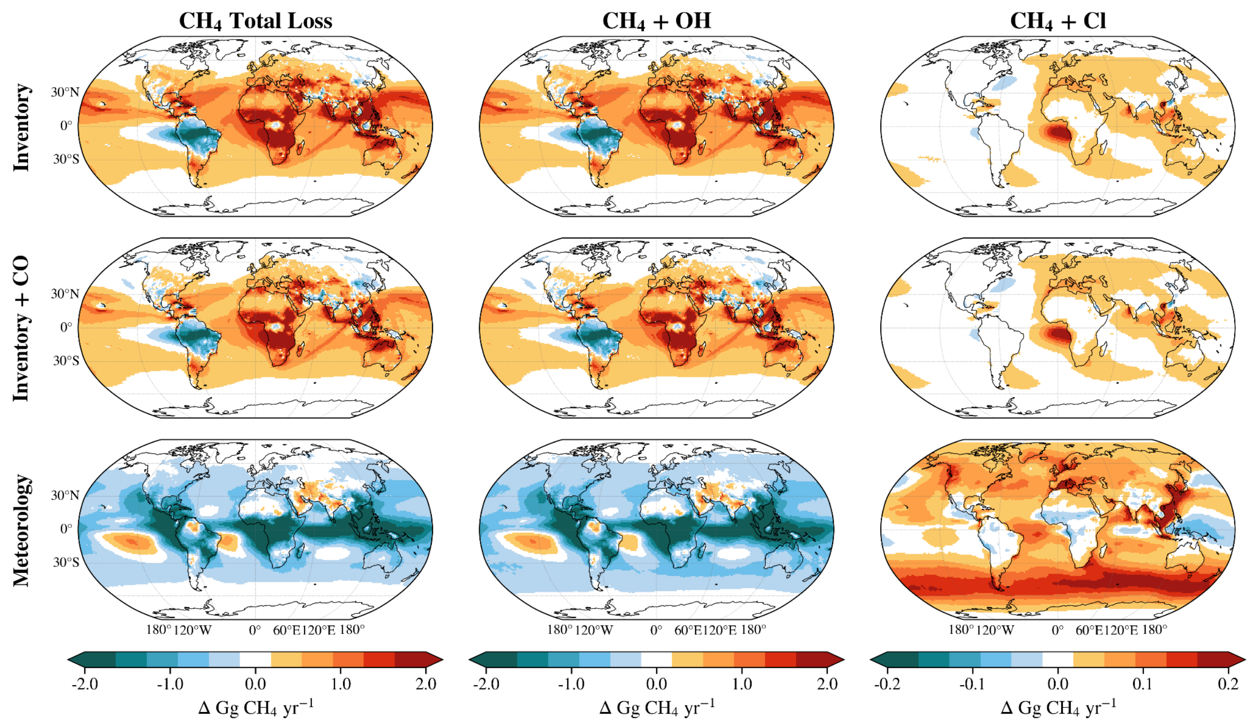

Figure S6. Climatological-mean (2003–2022) differences in CH_4 chemical loss between simulation pairs, isolating each driver: Inventory (CESM-CH4-CMIP7 − CESM-CH4), Inventory + CO (CESM-CH4-CMIP7-CO − CESM-CH4), and Meteorology (CESM-CH4-CMIP7-CO-ERA5 − CESM-CH4-CMIP7-CO). Columns show total CH_4 loss, CH_4 + OH and CH_4 + Cl.

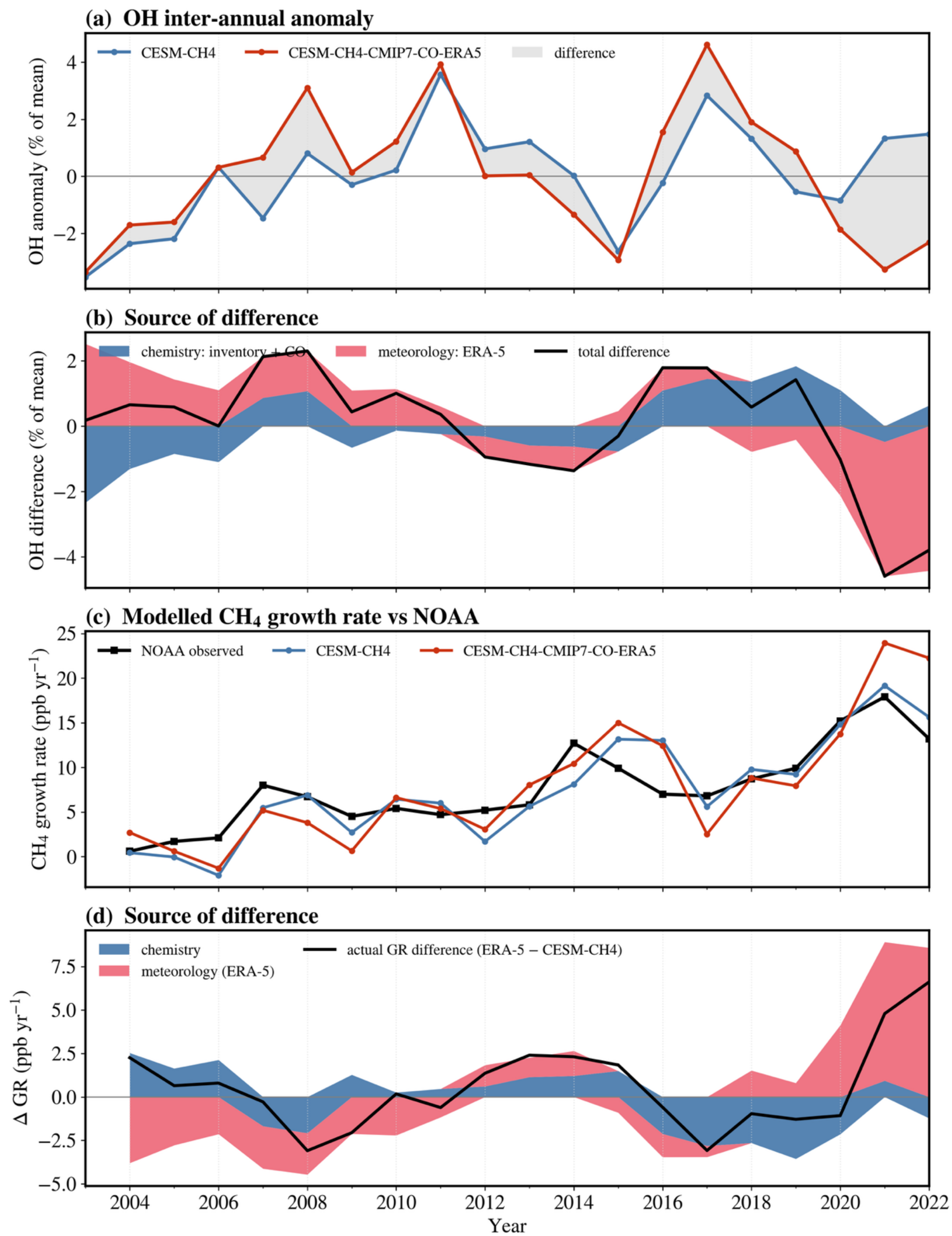

Figure S7. (a) OH inter-annual anomaly of the two best configurations and their difference; (b) the difference decomposes into chemistry (inventory + CO) and meteorology (ERA-5); (c) modelled CH_4 growth rate against NOAA; (d) the actual growth-rate spread against the contribution split into chemistry and meteorology.

S1. Methane-loss-weighted OH

A methane-loss-weighted (air-mass-weighted) OH, following Lawrence et al. (2001) is considered in this study. The domain is divided into four zonal bands , northern extratropics (NET, 30–90°N), northern tropics (NT, 0–30°N), southern tropics (ST, 30°S–0) and southern extratropics (SET, 90–30°S) and each band (*r)* is given a weight equal to its share of the global CH_4+OH loss,

$$w_r = \frac{L^{-}_{r}}{\sum_{r'} L^{-}_{r'}},$$

where L^{-}_{r} is the time-mean tropospheric CH_4+OH loss in band r. The global loss-weighted OH anomaly is then

$$OH'(t) = \sum_{r} w_r \, OH'_r(t)$$

with OH'_r the band-mean OH anomaly. We repeat the analysis with two alternatives, an air-mass weighting (using the well-mixed CH_4 burden as an air-mass proxy) and an OH-burden weighting and find that the regional weights stay tropically dominated and the global driver ranking is essentially unchanged in both configurations

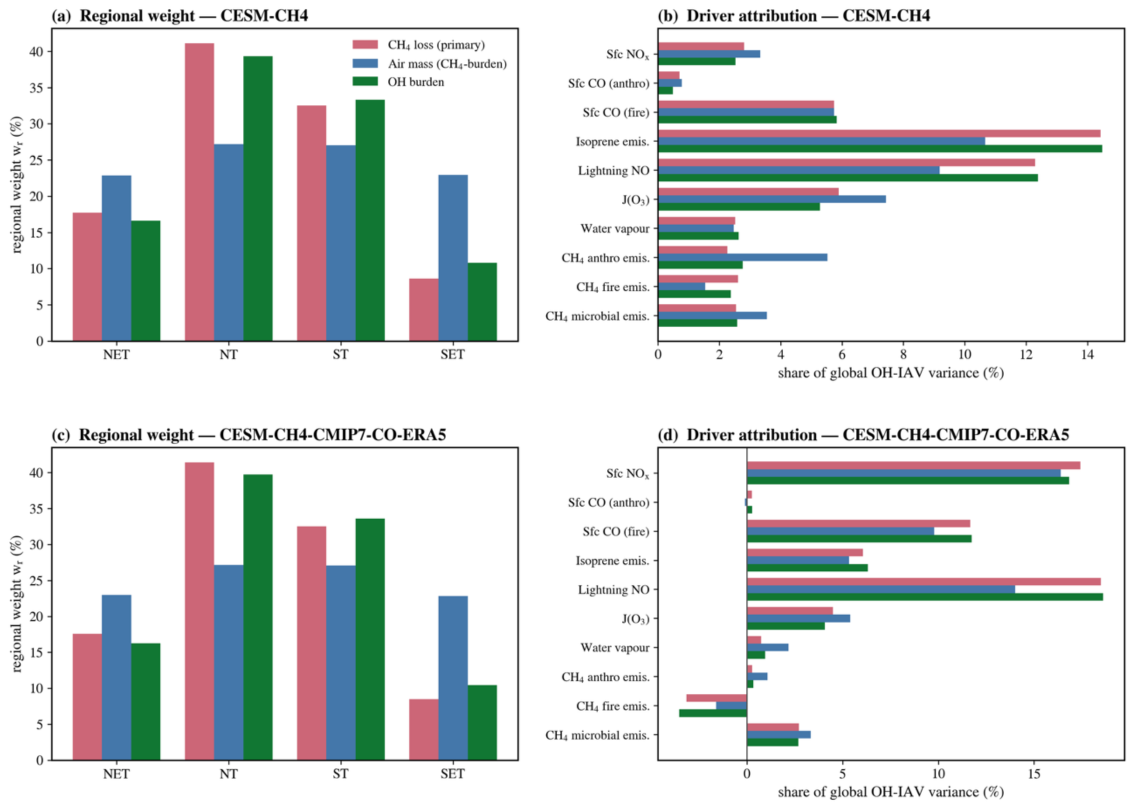

Figure S8. Weighting sensitivity of the attribution. Rows are the two configurations; the left column shows the regional weight w_r under the three weighting choices (CH_4 loss, air mass and OH burden), and the right column the resulting global driver shares

S2. Regional regression and aggregation

Within each band the OH anomaly is regressed on the local anomalies of a set of drivers by ordinary least squares,

$$OH'_r(t) = \sum_d \beta_{r,d}\, D'_{r,d}(t) + \varepsilon_r(t),$$

where $D'_{r,d}$ is the deseasonalised, anomaly of driver d in band r), OH'_r the corresponding detrended OH anomaly, and $\beta_{r,d}$ its sensitivity. The per-band sensitivities are independent of the weighting; the weights enter only in aggregating the bands to the global scale. The global contribution of driver *d* is the loss-weighted sum of its band-level contributions,

$$G_d(t) = \sum_r w_r\, \beta_{r,d}\, D'_{r,d}(t),$$

and the reconstruction of the global anomaly is the sum over drivers.

$$\widehat{OH}'(t) = \sum_d G_d(t)$$

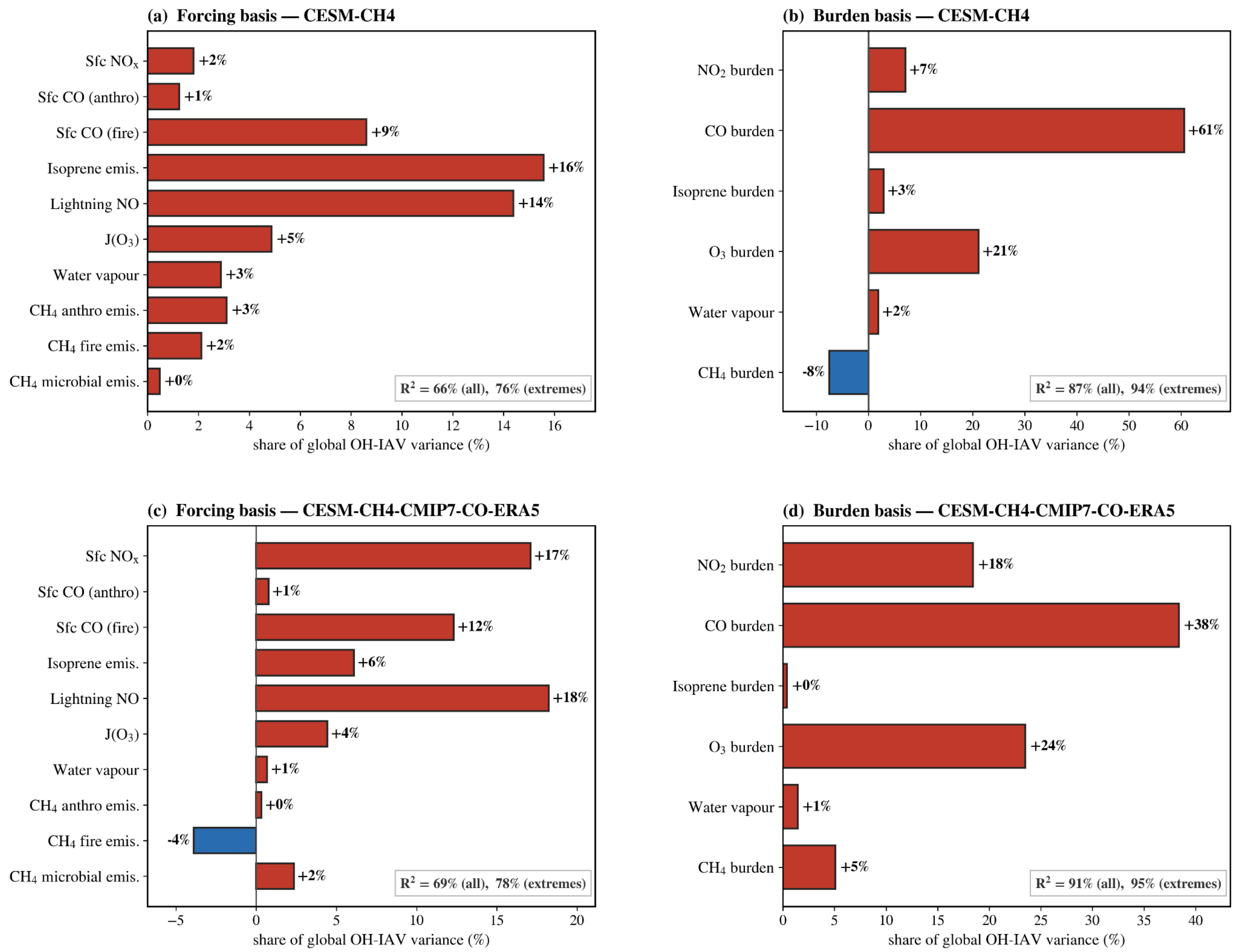

Figure S9. Driver attribution of the global OH-IAV variance for the two configurations (rows: CESM-CH4, top; CESM-CH4-CMIP7-CO-ERA5, bottom) in the forcing (left) and burden (right) bases, with reconstruction R^2.

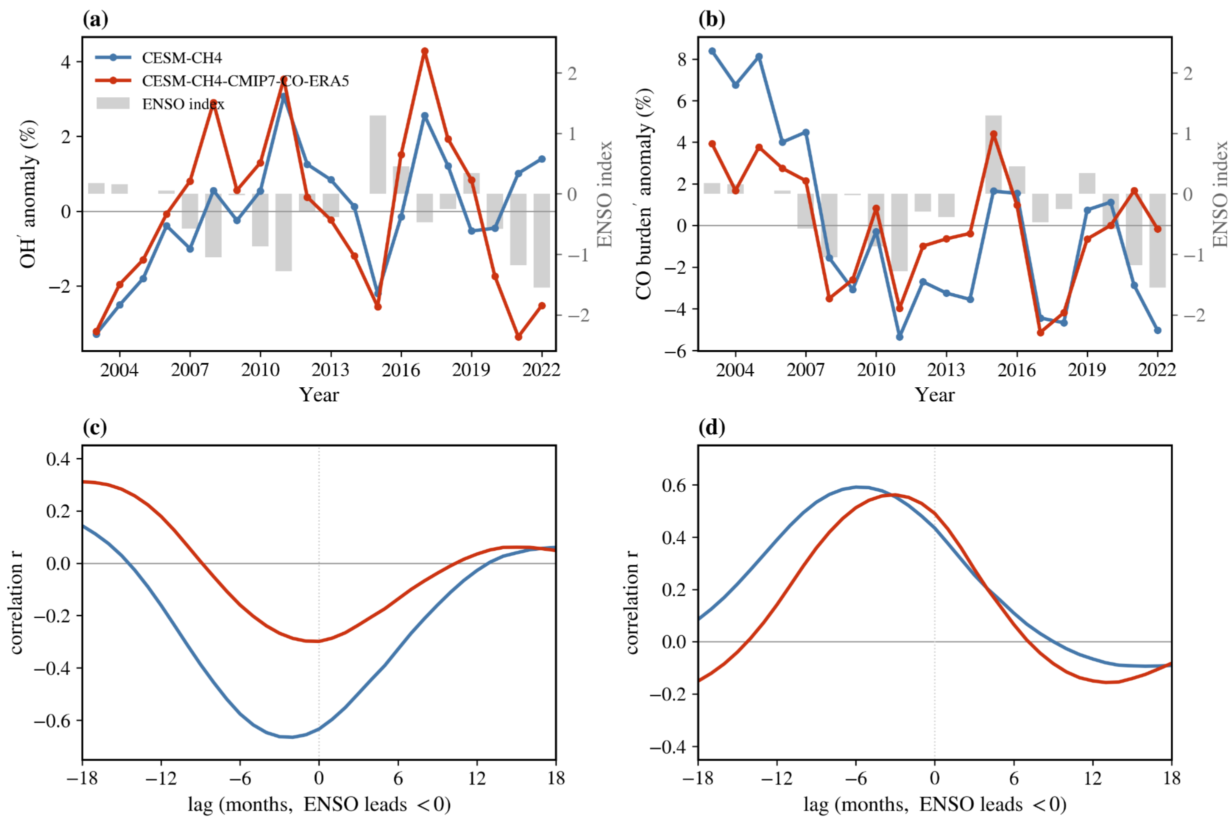

Figure S10. OH and CO-burden anomalies versus the ENSO index (MEI.v2), 2003–2022, for CESM-CH4 (blue) and CESM-CH4-CMIP7-CO-ERA5 (red). (a, b) Annual anomalies of (a) OH and (b) the CO burden (% of the 2003–2022 mean; left axes) with the ENSO index (grey bars, right axes). (c, d) Lead–lag cross-correlation of the monthly (c) OH and (d) CO-burden anomaly with the ENSO index (negative lag: ENSO leads).

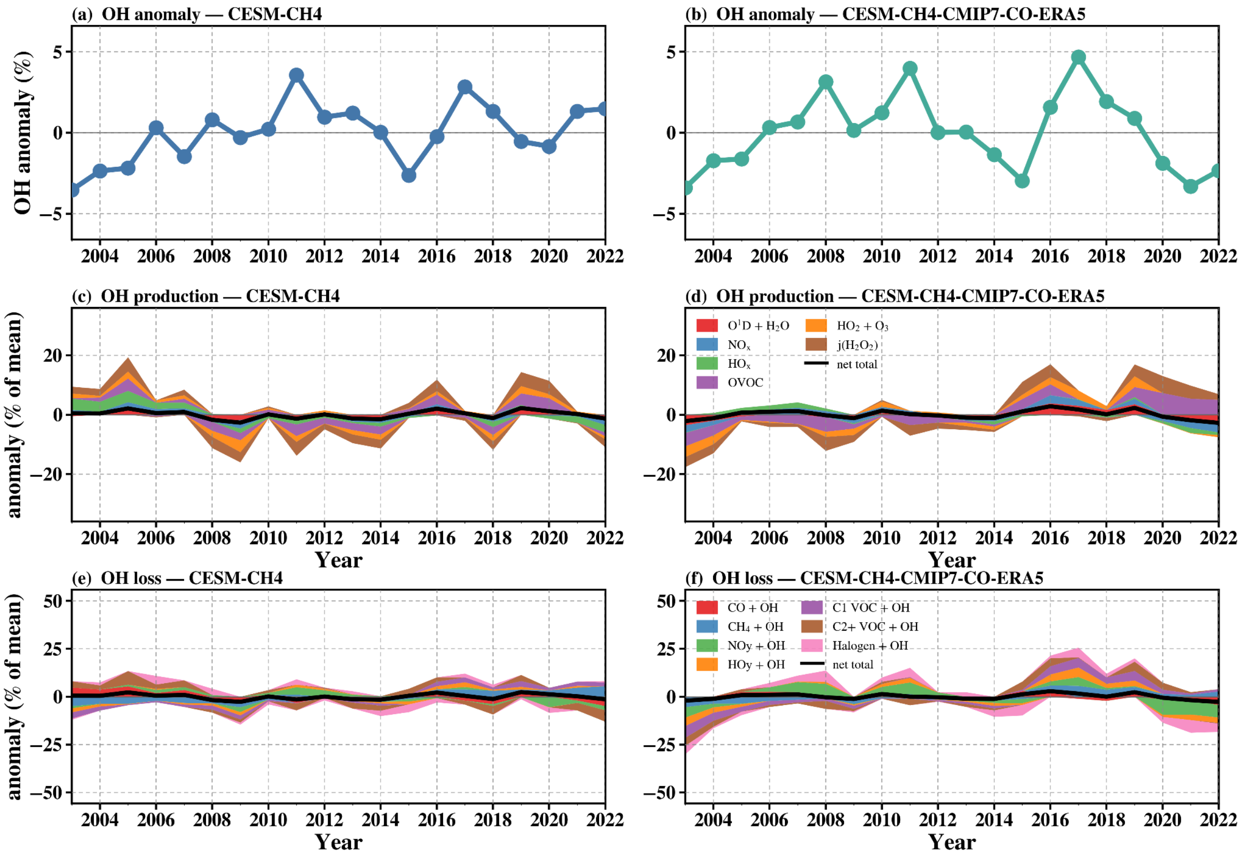

Figure S11. Tropospheric OH budget over 2003--2022 by reaction channel (detrended annual anomalies), for CESM-CH4 (left) and CESM-CH4-CMIP7-CO-ERA5 (right). (a, b) OH anomaly (%); (c, d) production and (e, f) loss channels (%), stacked about zero with the net as the black line.